Metabolic modeling of a plant-pathogen interaction quantifies the metabolic bottlenecks underlying bacterial wilt

Léo Gerlin[1,2], Stéphane Genin[1], Caroline Baroukh[1]*

[1]LIPME, Université de Toulouse, INRAE, CNRS, Castanet-Tolosan, France

[2]INRAE, INSA Lyon, BF2I, UMR203, 69621 Villeurbanne, France

*Corresponding author: caroline.baroukh@inrae.fr

ORCID: 0000-0002-1041-1730 (CB)

ORCID: 0000-0003-2498-2400 (SG)

ORCID: 0000-0002-1398-2790 (LG)

Keywords

Genome-scale metabolic model; plant-pathogen interaction; tomato; *Ralstonia solanacearum;* putrescine

Abstract

During plant infection, complex metabolic interactions take place between the plant and the pathogen, among which occurs a true battle for resources. On one side, the pathogen harvests nutrients at the expense of the plant to sustain its growth and virulence. On the other side, the plant tries to prevent pathogen multiplication by competing for nutrients or using anti-microbial compounds. Plants and pathogens have thus contrary objectives in an intertwined system that is particularly difficult to untangle experimentally. To help decipher this interaction, we used genome-scale metabolic modeling by combining a multi-organ model of a plant, a model of a pathogen, quantitative data and a mathematical approach using sequential flux balance analyses (FBAs). We applied this modelling strategy to the interaction between the pathogenic bacterium *Ralstonia pseudosolanacearum* and its natural host the tomato plant. This allowed, for the first time, quantitative modeling of the fluxes of matter occurring during plant infection. The model showed that, for the pathosystem studied, i) the plant's photosynthetic capacity is a more stringent environmental condition than minerals for bacterial proliferation ii) reduction of the plant transpiration is what limits and then stops plant growth and later pathogen growth, iii) hijacking stem resources can boost bacterial growth but is accessory, and iv) pathogen-excreted putrescine is predicted to be directly reused for plant biomass. This study provides the first holistic and quantitative view of a plant-pathogen interaction, and highlighted the criticality of water flow when the bacteria responsible of the infection is a fast-growing, xylem-colonizing one.

Significance statement

When a plant is infected by a pathogen, a true battle for resources occurs between the two organisms. On one side, the pathogen harvests nutrients at the expense of the plant to sustain its growth and virulence. On the other side, the plant tries to prevent pathogen multiplication by competing for nutrients or using anti-microbial compounds. To help understand this complex metabolic interaction, we used mathematical modelling to model both *Ralstonia pseudosolanacearum* and tomato plant metabolism.

This allowed, for the first time, a quantitative insight on metabolic interactions and consequences on physiology of the plant during an infection. Among other results, the model showed that plant transpiration decline is what limits and then stops plant growth and later pathogen growth.

Introduction

Metabolism is a determining parameter at the center of interactions between plants and pathogens. Indeed, during host infection, pathogens must efficiently find resources in hostile (and sometimes nutrient-poor) environments to sustain both their growth and virulence (Abu Kwaik & Bumann, 2013). This implies a trade-off for the infecting pathogen, which must balance its carbon and energy expenditure between two objectives: on one hand, limiting plant defense and hijacking plant resources, and on the other hand, supporting its own multiplication and proliferation (Berger et al., 2007). On the plant side, a similar trade-off exists where the plant must distribute resources between maintenance/growth (to ensure reproduction) and immunity, while coping with an increasing infecting population that affects its physiology (Herms & Mattson, 1992; Walters & Heil, 2007). Understanding this complex metabolic interaction between the plant and the pathogen is necessary to gain a more holistic view of the infection process. However, several challenges complicate this understanding: (i) the difficulty in distinguishing pathogen metabolism from plant metabolism, except for very specific metabolites, and (ii) the dynamic interplay of multiple synthesis and degradation processes. These factors prevent the use of a simple metabolomic comparison between infected and non-infected plants. To better tackle this complex interaction, a systemic and computational approach is necessary.

To address these challenges, genome-scale metabolic models (GSMM) could be used. GSMMs integrate the metabolic potential of an organism of interest, encompassing thousands of metabolic reactions based on genomics, physiological and biochemical evidences. These models can quantitatively predict the flux of matter in the biological system studied (Gu et al., 2019) as well as phenotypic parameters such as growth. GSMMs have repeatedly proven to be pertinent tools for unraveling complex metabolism and understanding it quantitatively, making them suitable for elucidating plant - pathogen metabolic interactions (Gerlin, Frainay, et al., 2021).

Recently, genome-scale metabolic modeling has been applied to the plant – pathogen system of tomato and *Phytophthora infestans* (Rodenburg et al., 2019). However, this study was only qualitative rather than quantitative. A quantitative model of the plant – mutualist symbiont system *Medicago truncatula* - *Sinorhizobium meliloti* has also been recently developed (diCenzo et al., 2020). Yet modeling a pathogenic interaction, as compared to a mutualistic one, raises additional methodological questions: (i) the

choice of the objective function (i.e. the flux(es) to minimize/maximize) in an antagonistic relationship, given that the modeling approach assumes an optimal behavior of the biological system; (ii) the need for extensive data acquisition, including the plant/pathogen ratio, growth rates, and metabolites available for the pathogen. These considerations are crucial for developing accurate, meaningful and quantitative models of plant-pathogen interactions.

In this study, we constructed the first quantitative genome-scale metabolic model of a plant–pathogen interaction. For our model pathosystem, we used *Ralstonia pseudosolanacearum* GMI1000 and its natural host, the tomato plant. *R. pseudosolanacearum* is a bacterial plant pathogen that has been extensively studied for its virulence factors (Vailleau & Genin, 2023) and has gained growing attention for the metabolic aspects of its lifestyle (Peyraud et al., 2016; Lowe-Power et al., 2018; Lowe-Power et al., 2018; Peyraud et al., 2018; Hamilton et al., 2021; Gerlin, Escourrou, et al., 2021). It was among the first plant pathogens having a high-quality genome scale metabolic model published (Peyraud et al., 2016). *R. pseudosolanacearum* is a soil-borne beta-Proteobacterium that enters plants through roots to reach the vascular tissues. The pathogen is then able to reach aerial parts, and proliferate dramatically in xylem vessels, which are typically considered nutrient-poor environments (De La Fuente et al., 2022). Bacterial density has been identified as for the cause of xylem vessel clogging (Ingel et al., 2022), leading to lethal wilting symptoms. A progressive growth arrest of the plant has also been observed (Gerlin, Escourrou, et al., 2021). The tomato, as *R. pseudosolanacearum*'s natural host, has also benefited from the recent growing importance of metabolic models in plants (Gerlin, Frainay, et al., 2021): a cell genome-scale metabolic model was originally published in 2016 (Yuan et al., 2016) and a genome-scale multi-organ metabolic model, with particular emphasis on xylem vessels (where *R. pseudosolanacearum* is most metabolically active), was recently published (Gerlin et al., 2022). A core metabolic model of tomato stem in the context of a fungal infection has also been published (Lacrampe et al., 2024).

In this study, we developed a quantitative genome-scale metabolic model of *R. pseudosolanacearum* – tomato plant interaction, named VIRION (VIrtual Ralstonia-tomato plant interactION). This model is based on the multi-organ metabolic model of the tomato plant, representing different plant organs during vegetative growth (leaf, stem, root with xylem and phloem as exchange compartments), and *R.*

pseudosolanacearum was added as an additional compartment connected to the xylem. To accurately simulate the antagonistic interaction between the plant and the pathogen, we employed a set of sequential Flux Balance Analyses (FBAs). VIRION also integrates a comprehensive set of physiological and metabolic data: i) tomato vegetative growth (organ ratio, growth rates, xylem metabolites), ii) tomato infection by *R. pseudosolanacearum* (plant/pathogen ratios, impacts of infection on physiology), and iii) *R. pseudosolanacearum* physiology and metabolic capacities (growth rates, assimilation and excretion capacities on xylem metabolites). The model enables the predictions of the growth capacities of *R. pseudosolanacearum in planta* at different stages of the disease, as well as the pathogen's impact on plant growth and metabolism. We used the model to analyze factors causing the infected plant to cease growth and those limiting bacterial growth. Finally, we also investigated potential hijacking of stem resources during the disease, and the fate of the bacterial excreted putrescine in the plant.

Results

Modeling an antagonist plant-pathogen interaction using a multi-compartment metabolic model and sequential Flux Balance Analyses

To quantitatively model the metabolic interaction between *R. pseudosolanacearum* and tomato, we formalized this interaction as a system composed of four metabolic compartments encompassing the main metabolic roles of the plant (leaf, stem, root) and the pathogen. Metabolites can be exchanged between these compartments through xylem and phloem (Figure 1A). Each of these four compartments was represented as genome-scale metabolic models: iRP1476 for the pathogen (Peyraud et al., 2016) and Sl2183 for the plant compartments (Gerlin et al., 2022) (Figure 1B), with minor modifications as reported in the Methods section. As in Gerlin et al. (2022), the physiological roles of each compartment (described in Figure 1A) were considered as FBA constraints (Figure 1B). In brief: i) minerals and water can only enter the system through the root and are routed to the higher parts of the plant and to the pathogen only via xylem, ii) photons are assimilated in leaf and stem, with higher efficiency in the leaf, iii) the carboxylase/oxygenase activity of the Rubisco was constrained to experimentally measured value. For a complete description and justification of these constraints, readers are referred to Gerlin et al. (2022).

FBA is an approach based on an optimization problem (typically linear programming), where one or several reactions must be maximized or minimized to compute fluxes of matter (Orth et al., 2010). Usually, when modeling ecosystems, it is assumed that the organisms composing the system maximize global biomass (diCenzo et al., 2020). However, this assumption is not reasonable for our antagonist system, where the pathogen grows at the expense of the plant, implying decoupled growth between the plant and the pathogen. Additionally, in our system, the metabolic composition of xylem sap is severely affected upon bacterial infection, particularly at high bacterial densities (Gerlin, Escourrou, et al., 2021), questioning the quasi-steady state assumption (QSSA). To accurately model this antagonistic relationship, we used a system of sequential FBAs (Figure 2). In this approach, an initial FBA determines one or several optimal flux(es). These fluxes are subsequently reinjected into a following FBA as an additional constraint. A total of 4 successive FBAs were performed for a given bacterial density to predict both bacterial and plant metabolism during the interaction. We

repeated this 4-FBA resolution workflow for several bacterial densities representative of those found *in planta*. This was achieved by changing the plant/pathogen ratio through exchange coefficients between the xylem and the pathogen.

The sequential 4-FBA approach consisted of the four following steps:

FBA 1: estimation of the requirements of a healthy plant in terms of photons, nitrogen and other minerals for optimal growth of leaf, stem and root.

FBA 2: optimization of pathogen growth while limiting plant photon input and optionally mineral inputs to those obtained in FBA 1. This ensured that resource usage did not exceed that of a healthy plant. Photon constraints were always applied, while iron, nitrogen or other minerals constraints were optional. Additionally, transpiration flow, which is significantly reduced after pathogen inoculation (Gerlin, Escourrou, et al., 2021) and affects xylem exchanges, could be constrained at this step.

FBA 3: integration of the pathogen's maximal growth obtained in FBA 2 as a constraint, while maximization of leaf and stem growth. This step estimated the plant's capacity to continue growth under the pathogen's metabolic activities. In both FBA 2 and FBA 3, root growth rate was constrained to experimentally observed values, as root growth is minimally affected by pathogen colonization of xylem vessels according to experimental data on infected tomato plants (Gerlin, Escourrou, et al., 2021).

FBA 4: minimization the sum of absolute fluxes while constraining leaf and stem growth rate to the optimal values obtained in FBA 3. This step represented a parsimonious enzyme usage by both the pathogen and the plant. This final simulation yielded the fluxes of matter and phenotype prediction (pathogen and plant growth) for a given bacterial density. By performing these 4 FBAs for bacterial densities ranging from 10^4 to 10^{12} Colony Forming Unit per gram of Fresh Weight (CFU/gFW), we captured all features of the plant-pathogen interaction during an infection. The simulation results were compared to experimental biological values to gain insights into the pathosystem.

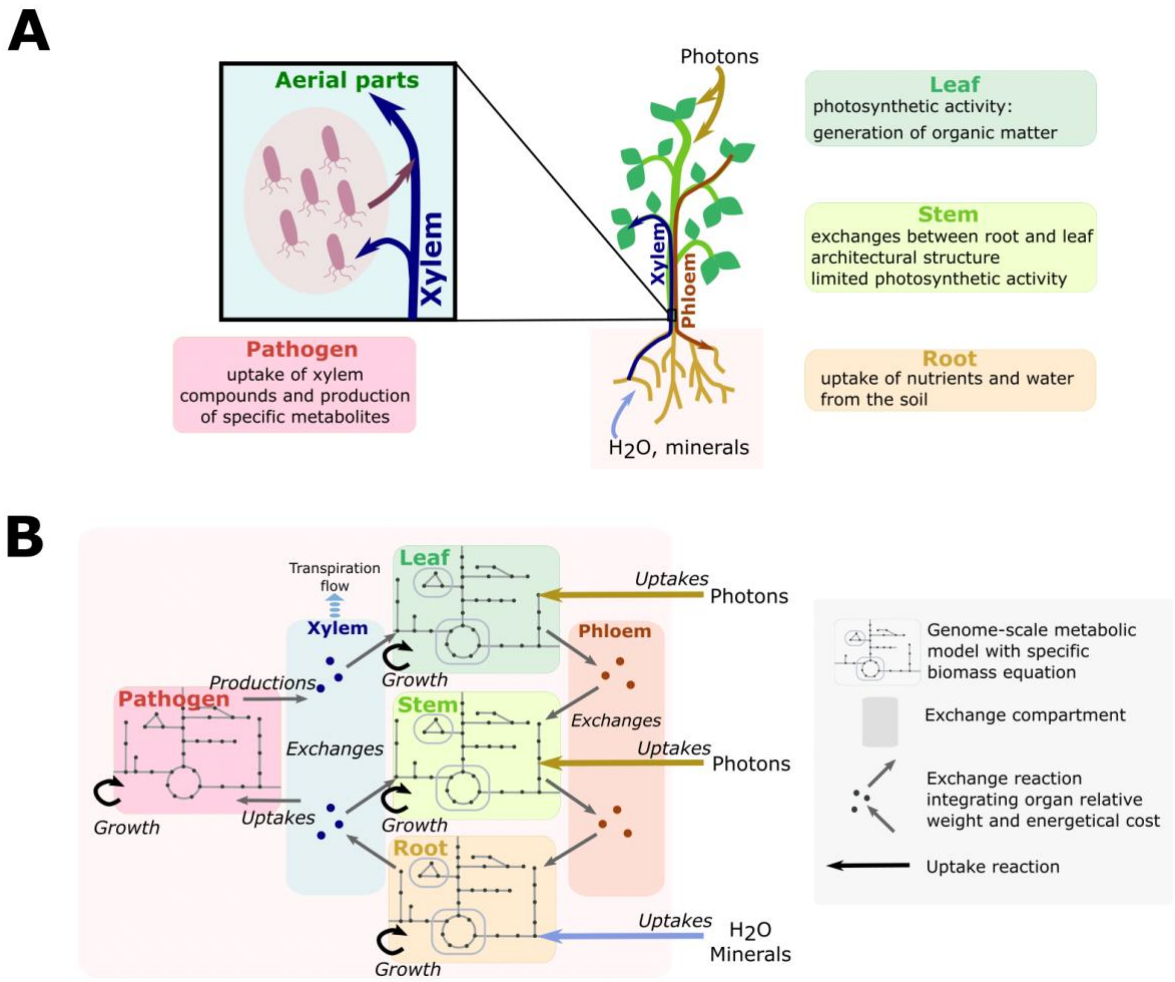

Figure 1: Schematic representation of the metabolic model VIRION

A. The main components of the system modeled in this study. Leaf, stem, root and the pathogen are each represented by a genome-scale metabolic model. Xylem and phloem are exchange compartments. Inputs of the system are photons, connected to leaf and stem, and water and minerals, connected through the root.

B. Schematic representation of the multi-compartment model and quantitative approach developed in this study. Arrows represent relationships between the different organs and the possible quantitative constraints which can be set in the model (growth, uptakes, exchanges, transpiration flow).

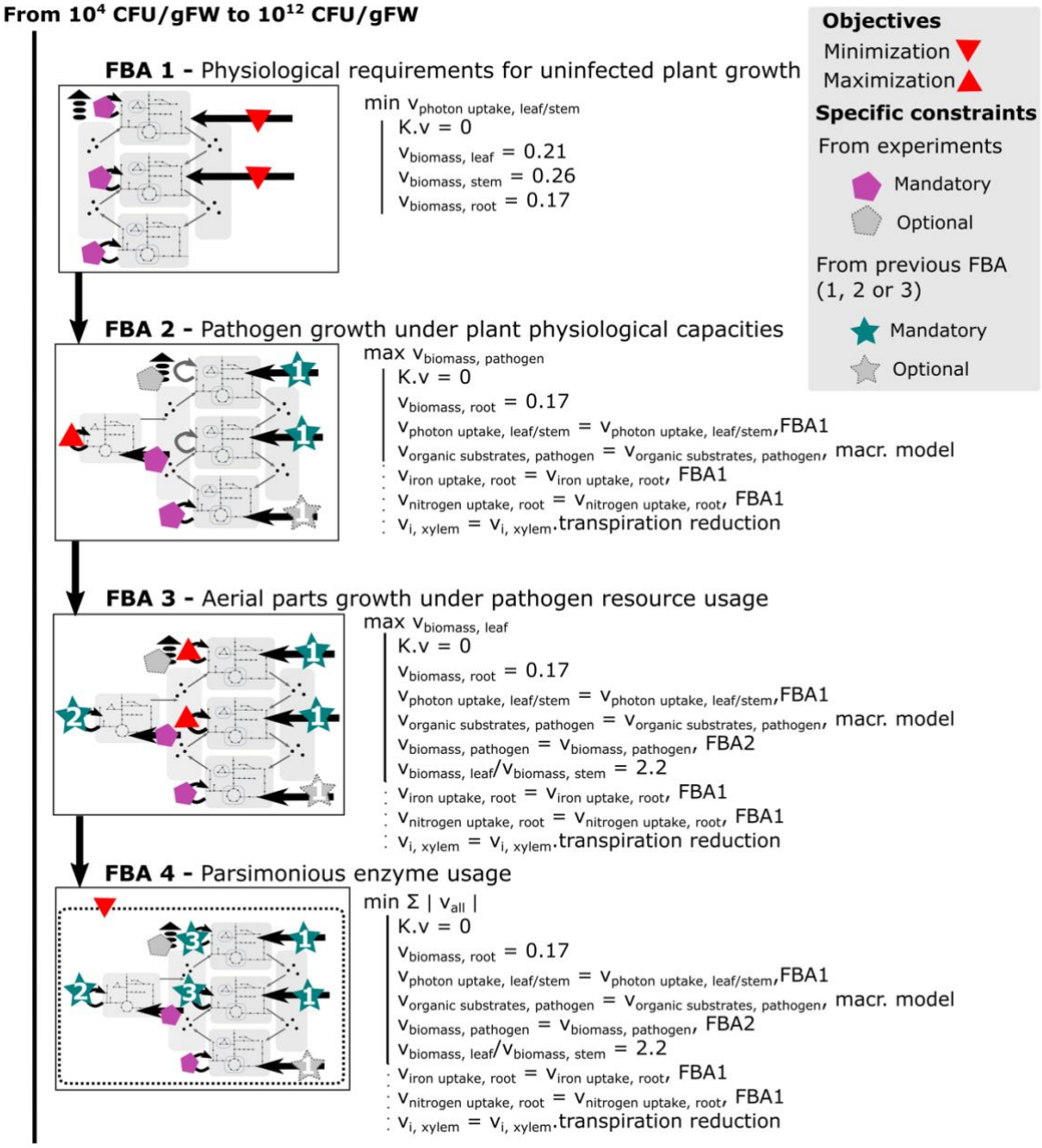

Figure 2: Sequential Flux Balance Analyses (FBAs). Schematic representation of the different FBAs solved in a sequential approach to obtain a phenotype prediction of the pathosystem (growth rate of plant organs and pathogen) as well as fluxes of matter. Dotted vertical lines represent optional constraints.See text for details.

Identifying metabolic bottlenecks during the plant – pathogen interaction

We used the VIRION model to estimate the most limiting plant environmental factor (bottleneck) constraining the plant – pathogen interaction. Our analysis focused on the effect of nitrogen, iron and transpiration as individual limitations or as combined constraints (Figure 3A). We considered photon limitation as mandatory since an infected plant could not increase its photons uptake. Indeed, the leaf area of an infected plant was similar or less than the one of a healthy plant (Gerlin et al., 2022). While other minerals could be tested, our study focused on nitrogen and iron, which are particularly emphasized in the literature. Indeed nitrogen source influences the concentration of xylem organic metabolites in tomato (Bialczyk et al., 2004), while both iron and nitrogen are suggested to influence bacterial switch to virulence in *R. pseudosolanacearum* (Bhatt & Denny, 2004; Dalsing & Allen, 2014; Dalsing et al., 2015). Iron and nitrogen limitations were implemented as constrained iron and nitrogen uptake rate in FBA 2 (maximizing pathogen growth, Figure 2), which could not exceed those inferred from FBA 1 (minimization of plant photons for a healthy tomato plant, Figure 2). In FBA 2, transpiration could also be limited in a proportional manner depending on the bacterial density using a previously determined linear relationship between *in planta* bacterial density and transpiration reduction established in Gerlin et al. (2021) (see material and methods for further details).

When photon availability is the sole limiting factor (Figure 3), which constrains photosynthesis and organic carbon production within the plant, *R. pseudosolanacearum* can grow at its maximal rate in the plant until a density of $10^{9.7}$ CFU/gFW (Figure 3B). Bacterial growth is then strongly reduced, reaching less than 0.05 h^{-1} when bacterial density exceeds $10^{10.6}$ CFU/gFW. We conclude here that plant carbon resources cannot support bacterial growth at higher density than 10^{10} CFU/gFW if bacteria growth relies solely on biotrophy.

Based on *in planta* analyses and *in vitro* assays on a mixture of substrates, glutamine has been characterized as the main carbon source of *R. pseudosolanacearum* in tomato xylem sap (Baroukh et al., 2022; Gerlin, Escourrou, et al., 2021; Baroukh et al., 2024). Our simulation results showed high glutamine uptake by *R. pseudosolanacearum* (Figure 3D), limited only by the bacterium's maximal uptake rate. At very high bacterial density, close to 10^{10} CFU/gFW, glutamine became insufficient

for both aerial part and bacterial growth, reaching the maximal allowed glutamine flux (Figure 3E), based on measurement for a healthy plant. This primarily impaired aerial parts growth, leading to a decline and then arrest of plant growth (Figure 3C), followed by limited *R. pseudosolanacearum* glutamine uptake and growth capacity. The glutamine limitation was slightly compensated by glucose uptake, a secondary carbon source co-consumed with glutamine. While glucose can moderately contribute to bacterial proliferation, it remains accessory (Baroukh et al., 2022, 2024; Gerlin, Escourrou, et al., 2021; Hamilton et al., 2021). At slightly higher densities ($10^{10.25}$ CFU/gFW), the maximal glucose flux in xylem was also reached (Figure 3G), further limiting bacterial growth (Figure 3F).

When comparing simulation results with only photon limitation to experimental data, plant physiological capacities were overestimated. Simulations showed optimal leaf and stem growth until a bacterial density of $10^{8.5}$ CFU/gFW (Figure 3C), whereas experimentally, a strong effect on plant growth occurred between 10^6 and 10^8 CFU/gFW (Gerlin, Escourrou, et al., 2021). This suggests that other factors are involved in the observed plant growth arrest. When minerals constraints (iron and nitrogen) were applied, separately or together, no additional effect was visible on plant and pathogen growths (Figure 3B and 3C) or metabolic exchanges (Figure 3D-G). This implies that nitrogen and iron were less stringent bottlenecks than carbon in the interaction. Replacing mineral constraints with a transpiration flow constraint resulted in a more drastic and earlier impact on growths (Figure 3B and 3C) and metabolic exchanges (Figure 3D-G). Reduction of transpiration, starting at 10^7 CFU/gFW, immediately limited xylem contents available for bacteria and aerial parts. Our sequential FBAs assumed that access to nutrients favors bacterial growth at the expense of plant growth. Consequently, the effect of transpiration limitation was immediate on plant growth (Figure 3C), which had access to less nitrogen. Transpiration limitation alone thus seems sufficient to provoke plant growth decline and eventual arrest, as observed experimentally. Following the impact on plant growth, xylem fluxes became insufficient to sustain the maximal growth rate of *R. pseudosolanacearum*, causing a switch to an intermediate growth rate (Figure 3B). However, xylem metabolites remained abundant enough to sustain this intermediate growth rate for several higher bacterial densities, as *R. pseudosolanacearum* can co-assimilate many available carbon sources (Baroukh et al., 2022, 2024).

Interestingly, up to 10^9 CFU/gFW, glutamine remained abundant enough to satisfy the glutamine maximal uptake rate of *R. pseudosolanacearum*. Other metabolites present at scarce concentrations in xylem, such as glucose (Figure 3F), sucrose and other amino acids (Supplementary Figure 1), were no longer assimilated or assimilated at reduced rate. Beyond 10^9 CFU/gFW, glutamine became insufficient for bacteria, strongly impairing its growth and leading rapidly to growth arrest. These findings align with experimental data, where the maximal CFUs are around 10^9 CFU/gFW (Gerlin, Escourrou, et al., 2021). They also corroborate with a recently developed macroscopic model of *R. pseudosolanacearum* growth *in planta* (Baroukh et al., 2024).

Finally, adding nitrogen and iron limitations to the model, which was already constrained by photons and transpiration, did not significantly alter the effect on disease progression (Figure 3B-G). This finding implies that the decline in transpiration of the plant, which reduces xylem fluxes, has the strongest effect on both plant and pathogen metabolic capacities. Transpiration decline thus seems to be the most probable mechanism behind plant growth arrest, pathogen growth arrest and maximal bacterial density. In contrast, limitations of nitrogen, iron and carbon (through photons) do not appear to be the primary mechanisms behind these experimental observations.

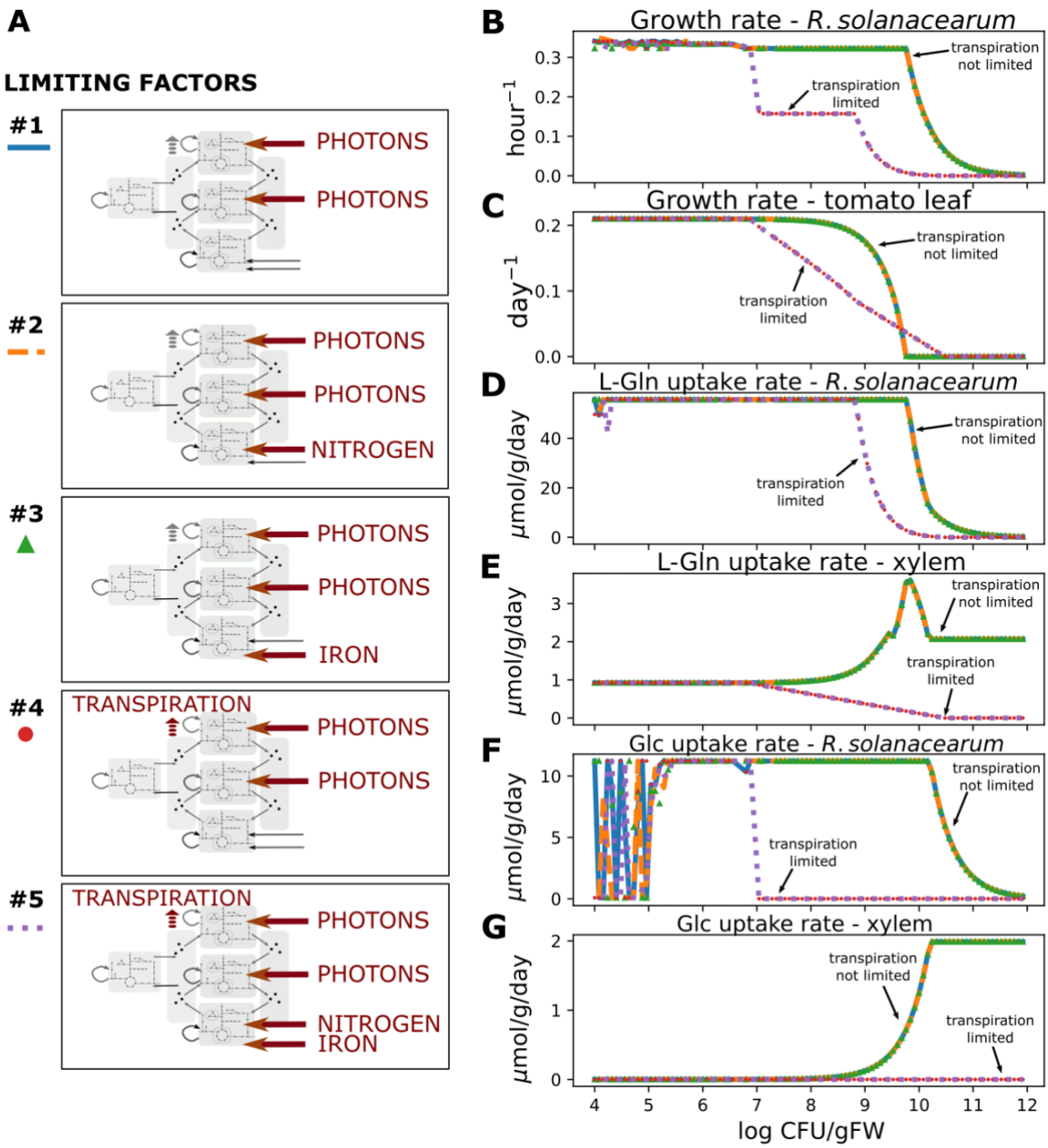

Figure 3: Effect of limiting plant environmental conditions on growth and metabolic exchanges. A. Simulation scenarios in which different plant environmental conditions are constrained at FBA 2 step during sequential FBAs. Photons, nitrogen and iron limitation constraints are set to the values obtained from resolution of FBA 1 while the transpiration limit is derived from experimental values (Gerlin, Escourrou, et al., 2021). B. to G. Effects of limiting factors on growth or exchanges for bacterial densities ranging from 10^4 to 10^{12} CFU/gFW. g means g of respectively *R. pseudosolanacearum* dry weight (D., F.) and root dry weight (E., G.). L-Gln: L-Glutamine, Glc: D-glucose, CFU: colony forming units, FW: fresh weight.

Quantitatively assessing the pathogen's strategy of hijacking tomato stem resources

In the previous simulations, contribution of stem to xylem sap was forbidden. This is consistent with the fact that no flux from stem to xylem was found by simulation for a healthy plant (Gerlin et al., 2022). However, it can be argued that these fluxes could appear in an infected tomato plant and thus contribute to pathogen nutrition if the pathogen uses a host resource hijacking strategy. This would align with the hypothesis that some type 3 secretion effectors of *R. pseudosolanacearum* modify plant metabolism (Landry et al., 2020; Macho, 2016). We re-modeled scenario #5 from the previous section (where photons, nitrogen, iron, transpiration are all limited, Figure 3A) but this time export of nutrients from stem to xylem was authorized (Figure 4A), creating scenario #6. Simulation results showed that allowing the stem to enrich xylem sap had a slight effect on tomato leaf growth (Figure 4C). However, a more important effect on pathogen growth was observed (Figure 4B). Indeed, Ralstonia could maintain a maximal growth rate until $10^{9.2}$ cells per g of fresh weight instead of 10^{7} in scenario #5, comparable to scenarios #1, #2 and #3 for which no transpiration limit was imposed (Figure 4B). The possibility to sustain a maximal growth rate at higher densities was due to the enrichment of xylem sap in glucose, sucrose and amino acids, thanks to the stem's contribution (Figure 4D, Figure 3, Supplementary Figure 1). Nutrients from the stem thus counterbalanced the effect of reduced transpiration flow and allowed *R. pseudosolanacearum* growth to reach higher densities. However, the capacity of the pathogen to induce such significant flux rewiring of the stem can be questioned since bacterial population dynamics *in planta* experimentally measured in Gerlin et al. (2021) agree more with scenario #4 or #5, in which no hijacking of stem resources occurs, as pathogen growth almost stops around 10^{9} cells per g of fresh weight.

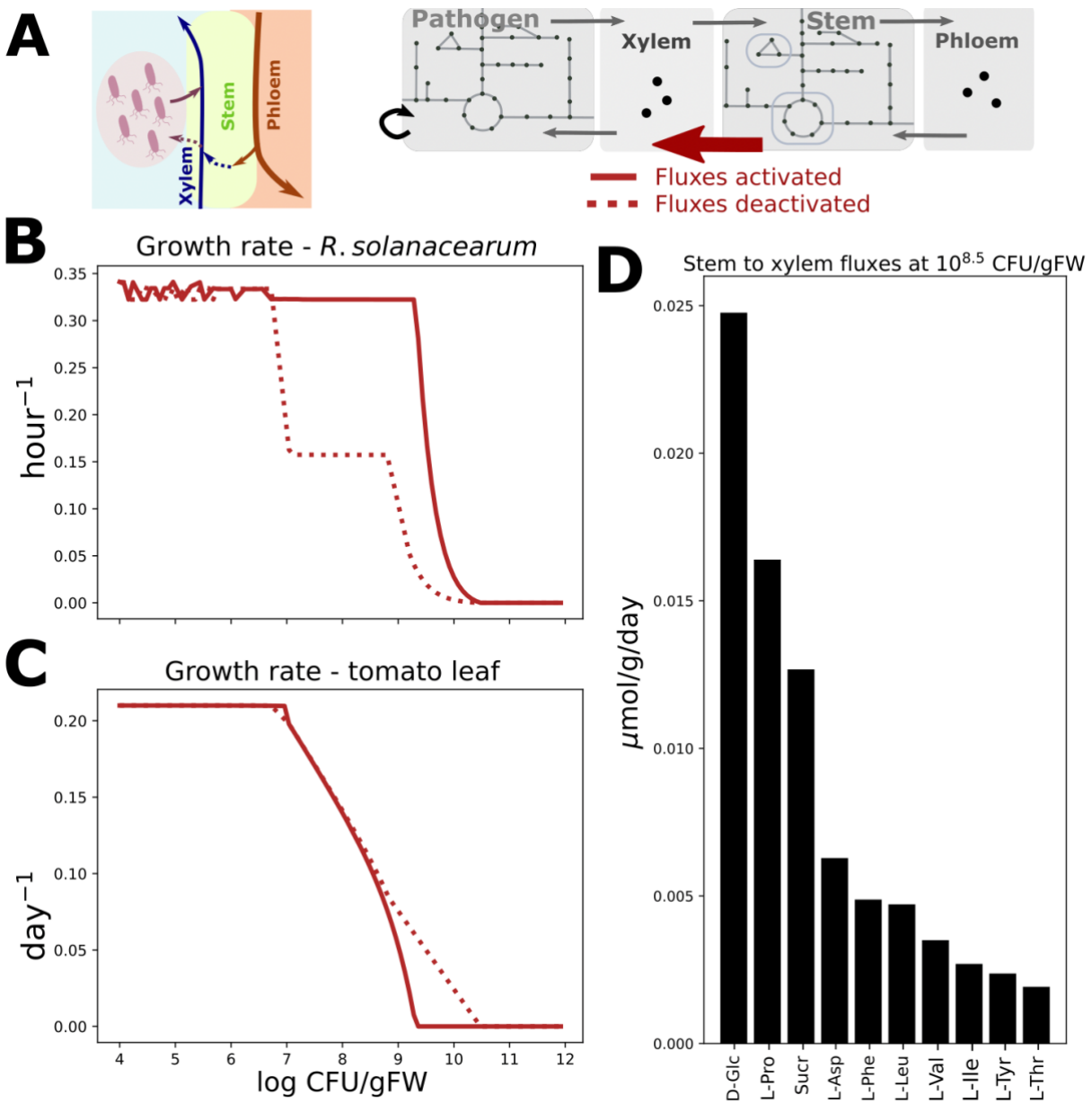

Figure 4: Effect of stem xylem sap enrichment on plant growth, pathogen growth and xylem sap composition. A. Schematic representation of the investigated plant fluxes. In scenarios #1 to #5, the stem could not enrich xylem sap. This rule was lifted to see the effect on the pathosystem metabolism. B. Pathogen growth rate when the stem can (dotted line) or cannot (line) enrich xylem sap. C. Plant growth rate when the stem can (dotted line) or cannot (line) enrich xylem sap. D. Fluxes of matter from stem to xylem when the stem can enrich xylem sap. g means g of stem dry weight. Fluxes were computed for a bacterial density of $10^{8.5}$ CFU/gFW. Fluxes are 0 when stem cannot enrich xylem sap. D-Glc: D-Glucose, L-Pro: L-Proline, Sucr: sucrose, L-Asp: L-Aspartate, L-Phe: L-Phenylalanine, L-Leu: L-Leucine, L-Val: L-Valine, L-Ile: L-Isoleucine, L-Tyr: L-Tyrosine, L-Thr: L-Threonine.

The fate of putrescine in the *Ralstonia*-tomato interaction

Putrescine fate during plant – *R. pseudosolanacearum* interaction is frequently questioned, as putrescine is abundantly produced by the bacterium *in vitro* and *in planta* (Gerlin, Escourrou, et al., 2021; Lowe-Power et al., 2018; Peyraud et al., 2016) and contributes to virulence by accelerating wilt symptoms (Lowe-Power et al., 2018). We analyzed the predicted fluxes in our model between putrescine production by *R. pseudosolanacearum*, quantitatively calibrated to its experimental putrescine excretion rate in a xylem mimicking media (Baroukh et al., 2024), and its assimilation by the plant, at a low and a high bacterial density ($10^{6.5}$ and $10^{8.5}$ cells per g of fresh weight) (Figure 5A). When putrescine is produced by the bacterium from ornithine, a small portion is incorporated into the bacterial biomass, while the majority is exported to xylem, following a previously characterized excretion rate (Baroukh et al., 2022, 2024; Peyraud et al., 2016). Subsequently, the plant stem has the capacity to assimilate part of this excreted putrescine. Some of the metabolic reactions associated with putrescine degradation were inactivated in our model, such as its conversion into N-acetylspermidine (R_RE1537C) or into N-Methylputrescine (R_PMT), since these fluxes would lead to dead-end metabolites not connected to central metabolism. Our model predicted that at low bacterial density, all putrescine is converted into 4-aminobutanal and then into gamma-Aminobutyric acid (GABA). The amount of GABA produced from putrescine at this bacterial density is inferior to the stem biomass requirements for GABA, which is supplemented by other reactions producing it from glutamate (R_GUDC, glutamate decarboxylase, 4.1.1.15). At high bacterial density, GABA production from putrescine exceed the stem biomass requirements. This excess of incoming putrescine is compensated by the activation of: i) the pathway allowing the incorporation of GABA into TCA cycle through GABA shunt (transport into mitochondria (R_4abut_tx_m_) and conversion into succinate-semialdehyde (R_ABTArm)) in the stem, ii) the activation of the pathway allowing conversion of putrescine into GABA and assimilation in biomass in the leaf. Interestingly, excess putrescine assimilated by the plant through GABA involves the mandatory production of hydrogen peroxide (H_2O_2) (Figure 5B), a modulator of redox homeostasis (Gerlin, Baroukh, et al., 2021), particularly in stem. The production of hydrogen peroxide in stem follows the pathogen growth, and peaks at 10^9 cells per g of fresh weight. At

higher densities, the limited capacities of the pathogen to pursue its growth impacts putrescine production flux, thus reducing hydrogen peroxide flux.

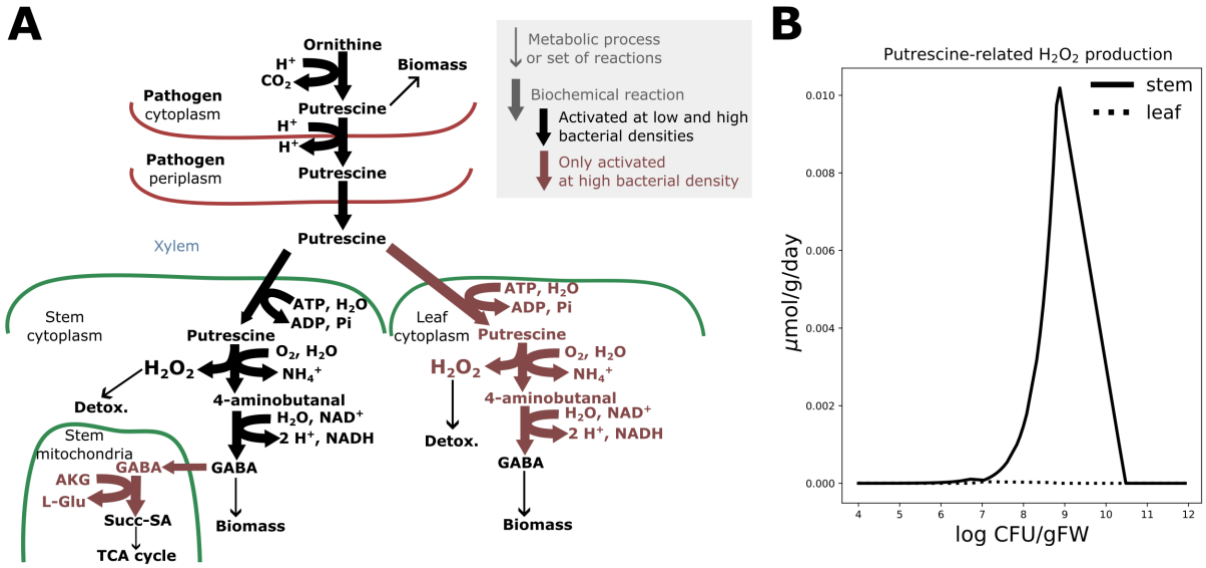

Figure 5: Fluxes predictions surrounding putrescine in VIRION. Only fluxes activated between putrescine production by the pathogen and its complete assimilation by the plant are represented. In B, g means g of stem (full line) or leaf (dotted line) dry weight.

Discussion

Modeling a plant-pathogen interaction using Flux Balance Analysis

FBA is a methodology widely used in the systems biology community because of its simplicity to set up, its capacity to model at the genome-scale level and its relatively low number of parameters to calibrate (Orth et al., 2010). However, this methodology relies on the quasi-steady-state assumption (QSSA), assuming that no internal metabolites of the system accumulate or get depleted, as well as the fact that the system is optimal with respect to an objective (most often assumed to be growth). The difficulty in modeling a plant-pathogen system lies in the fact that the pathogen grows at the expense of the plant, implying antagonistic objectives between the organisms composing the system. Therefore, questions arise regarding the choice of the objective function that should be optimized. In addition, the pathogen might deplete or accumulate some metabolites upon its growth in the plant, which probably challenges the QSSA.

As a first approximation to quantitatively model a plant-pathogen interaction, we proposed in this work a methodological framework consisting of solving, for several bacterial densities, 4 sequential FBA models in which each FBA model is constrained by the optimal value of the previously solved FBA. In this methodology, we thus assumed that for each bacterial density inside the plant, the internal metabolites were “at steady-state”. We also assumed that pathogen growth was at the expense of the aerial parts of the plant. Despite these strong hypotheses, VIRION was able to illustrate its relevance by predicting growth rates of the aerial part of the plant and the pathogen close to what was experimentally observed. VIRION also allowed to dissect novel and yet unquantified aspects of the *R. pseudosolanacearum* – tomato interaction, such as the importance of the transpiration decline and its implication in plant growth arrest, the importance of carbon compared to other elements and the relative importance of stem resource high-jacking.

As future directions, the model could be used to study the impact of plant environmental conditions on the plant-pathogen interaction or extended to consider plant defenses via the synthesis of anti-microbial compounds and the resulting bacterial mortality. From a methodological point of view, the QSSA could be slightly

relaxed on the metabolites composing the xylem sap, which would allow for more dynamic and relevant modeling of the plant-pathogen interaction.

Using mathematical modeling to better understand bacterial wilt disease

Since 2016, several mathematical models have been developed to better understand the biology behind bacterial wilt disease. The first model, released in 2016, consisted of a high-quality metabolic network of *R. pseudosolanacearum* simulated in diverse *in vitro* environments using FBA (Peyraud et al., 2016). This model allowed measuring the ATP- equivalent cost of EPS synthesis and virulence. This metabolic network was subsequently interfaced with a regulatory network controlling multiple virulence factors and simulated across a broad set of environmental conditions using a discrete logical modeling method (Peyraud et al., 2018). The resulting model revealed that the virulence regulatory network exerts a control of the primary metabolism to promote robustness upon infection.

More recently, Baroukh et al. (2024) modeled the *in planta* population dynamics of *R. pseudosolanacearum* during tomato infection using a macroscopic modeling framework relying on Monod kinetics. This mathematical model predicted substrate consumption, putrescine production and biomass growth of *R. pseudosolanacearum*. Unlike previous models, it did not incorporate the metabolic network of *R. pseudosolanacearum* or its regulatory network, nor did it include the plant's metabolic network, which was simply modeled as a continuous environment providing substrate fluxes to the pathogen. Despite these simplifications, the model accurately reproduced experimental observations, including high bacterial densities and the depletion of glutamine and asparagine. Additionally, it estimated key parameters such as the bacterial mortality rate within the plant and the rate at which bacterial putrescine is assimilated by the plant.

In the present study, the metabolic networks of *R. pseudosolanacearum* and the tomato plant were merged, and the resulting model was simulated using sequential FBAs for diverse bacterial densities within the plant. The model demonstrated several key findings: i) the plant's photosynthetic capacity is the most critical factor for bacterial proliferation, ii) a reduction in plant transpiration limits and ultimately stops plant and pathogen growth, iii) hijacking stem resources, potentially through virulence factors,

can enhance bacterial growth but is not essential, and iv) pathogen-excreted putrescine is predicted to be directly reused for plant biomass.

Another metabolic model of a plant-pathogen interaction was recently developed by Rodenburg et al. (2019), representing the *Phytophthora infestans* - tomato leaf pathosystem. This study differs from ours in several key aspects, as it employs a qualitative approach, in contrast to our quantitative methodology. This difference is evident in: i) The *P. infestans* biomass equation, which uses equal stoichiometric coefficients, ii) The absence of mass conversion between plant and pathogen fluxes iii) The unrestricted uptake of all metabolites from tomato cell cytosol by the pathogen, and iv) The lack of calibration for maximal uptake rates for both *P. infestans* and the plant. Roderburg et al. (2019) also utilized a tomato leaf-centered model, which is substantially less complex than our multi-organ model that incorporates a vascular system, and the impact of *P. infestans* growth on plant metabolism and physiology was not simulated. Indeed, all objective functions in their FBA simulations focused exclusively on pathogen growth, whereas our model considers the interplay between pathogen and plant growth.

In each of the Ralstonia mathematical models developed so far, different modeling approaches have been used, different objects have been modeled, various experimental data have been used for calibration, and distinct biological questions have been addressed. Consequently, each model possesses its own specificity and provides unique insights into the mechanisms at play during bacterial wilt disease. Future directions could involve improving existing models by better representing the plant putrescine degradation pathway and incorporating the synthesis of anti-microbial compounds. Alternatively, models could be made more complex by considering the spatial aspects of infection and representing the effects of abiotic and biotic conditions of the plant on the pathosystem.

Plant transpiration is the main factor leading to growth arrest of both the host and the pathogen wilt disease

VIRION allowed to test and identify which physiological or environmental factors are behind plant growth arrest and pathogen growth arrest during bacterial wilt disease. First, our simulation results showed that the maximal carbon uptake capacity of the plant (through photosynthesis), not nitrogen or iron, set the maximal plant density of Ralstonia cells achievable (Figure 6). However, we also found that carbon, or any other

metabolic bottlenecks such as nitrogen and iron, are insufficient to explain the early arrest of plant growth that was experimentally observed in Gerlin et al. (2021). To explain this plant growth arrest, a physiological constraint was necessary: limiting transpiration, impacting xylem fluxes and hence access to nutrients for the plant aerial parts and later on the pathogen (Figure 6). Interestingly, at densities where this transpiration-limitation is induced, the plant growth was affected immediately, in agreement with experimental observations, contrary to the bacteria which continued to thrive up to several logs higher. This underlines the pathogen's perfect metabolic adaptation to this challenging environment.

Naturally, questions arise on the mechanism responsible of plant transpiration decrease upon *R. pseudosolanacearum* presence in xylem vessels. Physical presence of Ralstonia cells could impede xylem flow in itself, but an indirect mechanism such as large bacterial exopolysaccharides excretion could also be responsible by making xylem sap so viscous that it impedes its flow. To discriminate between these hypotheses or others possible mechanisms, further investigation is necessary.

Stem resource hijacking, a strategy likely little used by *R. pseudosolanacearum* during tomato infection

In literature, it is commonly described that xylem sap is nutrient-poor and cannot sustain the biotrophic growth of a plant pathogen to high densities (De La Fuente et al., 2022), thus requiring the bacterial pathogen to force the plant to release additional nutrients, such as sugars (Hamilton et al., 2021; MacIntyre et al., 2020). However, VIRION simulations tend to show that, even with a transpiration limit, a moderate growth rate of *R. solanacearum* can be reached up to 10^9 CFU/gFW solely through biotrophic growth, in agreement with experimental observed values (Gerlin, Escourrou, et al., 2021). From 10^{10} CFU/gFW, a growth rate is still present but very close to 0. Thus, xylem sap, when considered as the product of a continuous flow, is not poor and very high bacterial densities can be reached solely through biotrophic growth of the pathogen.

We then investigated how resource hijacking could contribute to *R. pseudosolanacearum* growth. We confirmed by simulation that this mechanism could theoretically be an effective pathogen strategy to boost its growth and compensate, for example, the effect of transpiration decline, since it allowed the pathogen to have a non-negligible growth rate up to 10^{10} CFU/gFW. We also confirmed that in the case of

stem resource hijacking, this would primarily involve sugars and some amino acids (Figure 6). This would explain why Hamilton et al. (2021) reported a slight increase of sugars in infected xylem sap. Nevertheless, we also showed that this mechanism is probably dispensable for *R. pseudosolanacearum* since according to bacterial population dynamics *in planta* experimentally measured in Gerlin et al. (2021), pathogen growth almost stops around 10^9 CFU/gFW and not 10^{10} CFU/gFW. This also aligns with the observation that mutants defective in sugar assimilation still fully wilt tomato plants, with a slight delay (Hamilton et al., 2021; Gerlin, Escourrou, et al., 2021). We thus conclude that hijacking plant resources from the stem is not likely to occur in bacterial wilt or, if it does, the quantities of nutrients hijacked are much lower than the maximal quantity that can be theoretically hijacked, as predicted by the model. Targeting glutamine which is the major carbon source for the bacterium, thus seems a better strategy to limit *R. pseudosolanacearum* growth in the plant. However, such modifications would likely affect plant metabolism and phenotype even before impacting the pathogen, as our model tends to indicate. Nevertheless, it might be worthwhile to consider how managing the plant's environment, such as nutrition or watering, could mitigate xylem sap flow and composition and thus minimize *Ralstonia* growth in the plant.

While *R. pseudosolanacearum* appears to favor a fast consumption of resources, as its metabolic and growth capacities outcompete those of the plant, other plant pathogen might not exhibit this behavior but instead favor a reduced growth in xylem vessels. In particular, *Xylella fastidiosa*, although capable of metabolizing various xylem sap components (Gerlin et al., 2020), has very limited growth rates *in vitro* and *in planta*, and is described as adopting a self-limiting behavior (Gerlin et al., 2020; Roper et al., 2019). In these conditions, the plant would be able to dominate the trophic interaction and limit bacterial spread. This suggests that these pathogens would favor a long stay in xylem vessels at low bacterial densities. In this case, a coexistence with the plant takes place in which the bacterium is not competing for resources, and both the plant and the pathogen can remain metabolically active.

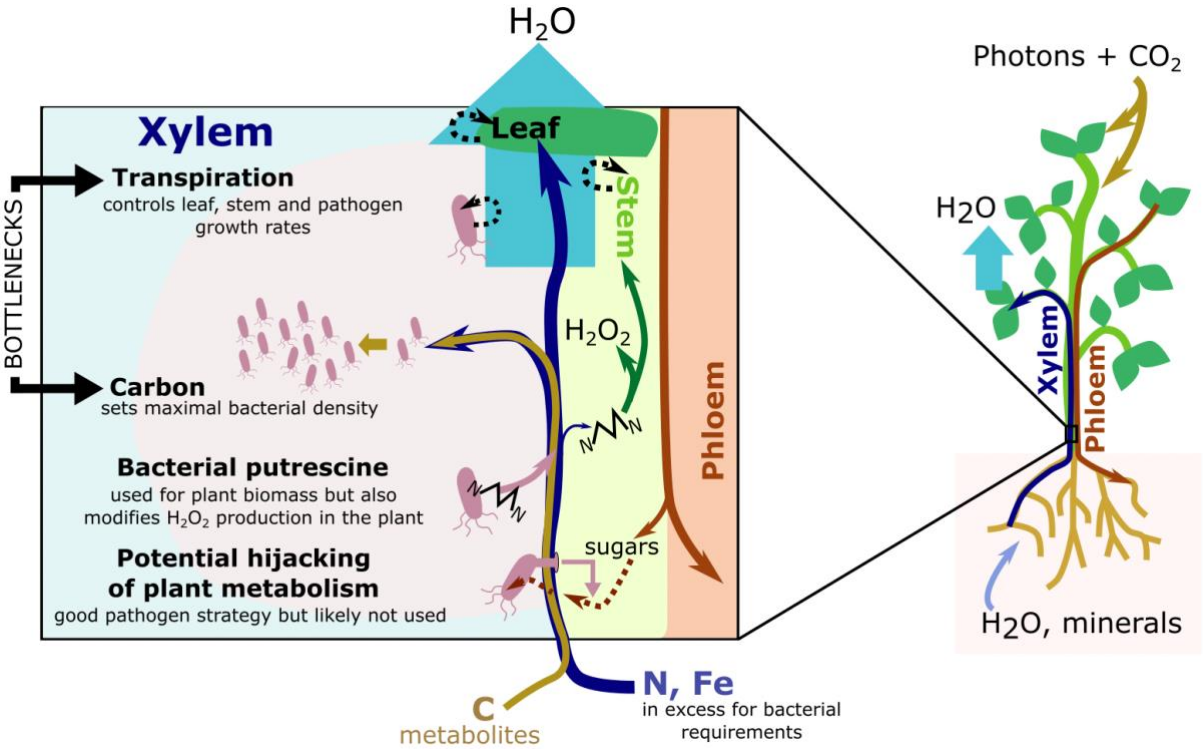

Figure 6: Key metabolic parameters during bacterial wilt at the origin of a successful infection. Decrease in transpiration during infection appears to be the most likely mechanism behind the cessation of plant growth and pathogen growth. Among diverse nutrients, carbon is the most limiting one for bacterial maximal density reachable. The study also shown that diverting nutrients from the phloem to the xylem via the stem is a good strategy to increase bacterial multiplication in the plant but poorly used in the case of bacterial wilt. Finally, the effect of bacterial putrescine production on host metabolism was shown to interfere with H_2O_2 synthesis in the plant, likely having an effect on ROS response.

Methods

Construction of VIRION

The cell tomato metabolic model from Gerlin et al., (2022) was used (SBML file) as a starting point. Reactions for iron, manganese, cobalt, molybdenum and zinc assimilation, which were not represented in the initial metabolic model, were added as these metabolites were necessary for predicting *R. pseudosolanacearum* growth using its genome-scale metabolic model (Peyraud et al., 2016). This addition, as well as other changes or improvements on putrescine metabolism and biomass are fully described in Supplementary Text 1. A multi-organ tomato model was generated using the same procedure as in Gerlin et al., (2022). Briefly, using an in-house script, the model was replicated into three models, representing leaf, stem and root with adequate biomass reaction for each organ. Exchange reactions, considering weight ratios between the different organs, were added to allow the exchange of metabolites between organs through xylem and phloem. Xylem represented exchanges between root and aerial parts, while phloem represented exchanges between aerial parts and roots. Stem could exchange in both directions with the phloem. Contrary to our previous multi-organ metabolic model, stem could uptake elements from the xylem but could not provide elements to this compartment, except when mentioned. As in Gerlin et al., (2022), a transport cost was added for each exchange reactions except for water. Different physiological constraints (uptakes of water and minerals by roots only, no photosynthesis for root, limited photosynthesis for stem) were integrated to model the different roles of each organ as in Gerlin et al., (2022).

The in-house scripts also merged *R. pseudosolanacearum* metabolic model taken from Peyraud et al. (2016) to the multi-organ model, generating a four-compartment model: leaf, stem, root, pathogen. The boundary metabolites were removed from the metabolic model of *R. pseudosolanacearum*, and external metabolites of the pathogen model were considered as xylem metabolites. To avoid dead-end metabolites, sink reactions were added allowing the exit of *R. pseudosolanacearum* metabolites excreted into the xylem and not present in healthy plant xylem sap. Simulations revealed very few sink reactions were used, and at very low fluxes. In addition, experimental data showed that few metabolites were enriched upon Ralstonia infection in xylem sap (Gerlin, Escourrou, et al., 2021; Lowe-Power et al., 2018). The weight

ratio between *R. pseudosolanacearum* and the plant was implemented in the exchange reactions between the xylem and the bacterial periplasm and were modified to represent the different bacterial densities. Conversion of *R. pseudosolanacearum* weight into colony forming unit (CFU) per g of fresh weight (FW) was estimated to follow 1 CFU/g stem FW = $1.10 \cdot 10^{-11}$ g bact / 1.52 g stem dry weight, based on: i) OD/CFU and OD/g ratios from Peyraud et al. (2016), ii) fresh weigh/dry weight (FW/DW) from Gerlin et al. (2022), iii) the leaf/stem and stem/root ratio in tomato metabolic model (Gerlin et al., 2022) which impose relative contents of 1.52 g stem DW and 3.37 g leaf DW for 1 g root DW (Supplementary Text 2).

Calibration of *R. pseudosolanacearum* metabolic model for growth *in planta*

To determine growth, excretion and assimilation capacities of *R. pseudosolanacearum* in the presence of xylem carbon sources, we used the data and model generated in Baroukh et al. (2024). In this study, a shake-flask growth experiment was performed in a minimal medium supplemented with a mixture of organic substrates whose relative concentrations mimics a tomato xylem. Growth, substrate assimilation and product excretion were monitored and used to determine uptake, excretion and growth rates among this combination of carbon sources. Glutamine and glucose assimilation followed Monod-type kinetics and were driving growth, while other substrate assimilation rates were proportional to the assimilation of glutamine and glucose. From the Monod kinetics, two maximal assimilation rates, one for glutamine and one for glucose, were implemented as a constraint bound in the model:

$$Gln_{ass_{rate}} \leq k_{gln} * \mu_{max_{gln}} * \frac{[Gln]}{[Gln] + K_{s_{gln}}} * 1000 * 24$$

$$Gluc_{ass_{rate}} \leq k_{gluc} * \mu_{max_{gluc}} * \frac{[Gluc]}{[Gluc] + K_{s_{gluc}}} * 1000 * 24$$

With:

- $Gln_{ass_{rate}}$ the assimilation rate of glutamine in the model (mmol.gB^{-1}.day^{-1}), k_{gln} (mmol.mgB^{-1}) the quantity of glutamine necessary to yield 1mg of biomass, $\mu\max_{gln}$ (h^{-1}) the maximal growth rate on glutamine, $K_{S_{gln}}$ (mM) the semi-saturation growth term on glutamine, $[Gln]$ (mM) the concentration of glutamine in tomato xylem sap

- $Gluc_{ass_{rate}}$ the assimilation rate of glucose in the model (mmol.gB^{-1}.day^{-1}), k_{gluc} (mmol.mgB^{-1}) the quantity of glucose necessary to yield 1g of biomass, $\mu\max_{gluc}$ (h^{-1}) the maximal growth rate on glucose, $K_{S_{gluc}}$ (mM) the semi-saturation growth term on glucose, $[Gluc]$ (mM) the concentration of glucose in tomato xylem sap

From each other substrate, to ensure assimilation only when glucose or glutamine were assimilated, a constraint proportional to glucose and glutamine rate was added:

$$os_{ass_{rate}} \leq \frac{k_{OS}}{k_{gln}} * Gln_{ass_{rate}} + \frac{k_{OS}}{k_{gluc}} * Gluc_{ass_{rate}}$$

With $os_{ass_{rate}}$ (mmol.gB^{-1}.day^{-1}) the assimilation rate of the other substrate (phenylalanine, valine, leucine, arginine, sucrose, tyrosine, proline, lysine, threonine, isoleucine, asparagine). All values were taken from Baroukh et al. (2024).

ATP maintenance was calibrated so that *R. pseudosolanacearum* growth rate prediction was in agreement with experimental data measured in Baroukh et al. (2024).

Sequential FBAs

Modeling of the interaction was performed using four successive FBAs with different objective functions.

1. Minimization of photon uptake

This first FBA is performed with leaf, stem and root growth rates constrained to experimental values, on the plant alone (VYTOP model). Minimizing photon uptake allowed acquiring the plant physiological capacities (photosynthesis, iron, nitrogen uptake) to ensure growth of a healthy plant in the absence of a pathogen.

2. Maximization of the pathogen biomass

The photon uptake rate determined in FBA 1 (representing healthy plant physiological capacities) was implemented as additional constraint, to avoid that the infected plant has a higher photosynthesis rate than a healthy plant. The leaf and stem growth rates were relaxed, to model the fact that *R. pseudosolanacearum* resource acquisition and proliferation will hinder the possibility of the aerial part of the plant to grow optimally, as observed experimentally (Gerlin, Escourrou, et al., 2021). Root growth rate remained constrained as we found in the experiments that root growth was not impacted by *R. pseudosolanacearum* (Gerlin, Escourrou, et al., 2021). The objective

function in this FBA was the maximization of the pathogen biomass reaction (i.e. maximal proliferation). The result of the simulation was the maximal growth rate of *R. pseudosolanacearum* constrained by the plant physiological capacities.

In this FBA, it was also possible to limit the nitrogen or iron uptake rate of the plant by setting the upper bound the related transport reactions to the value obtained FBA 1. It was also possible to limit transpiration. Measurements of transpiration during plant – *R. pseudosolanacearum* interaction revealed a decrease of transpiration when the pathogen is present at more than 10^7 cells per g of stem fresh weight (FW) (Gerlin, Escourrou, et al., 2021). We estimated thanks to a linear regression a transpiration decrease linear rule, depending on the bacterial density (in decimal logarithm): $t_{ranspiration\ reduction\ coefficient} = -0.2746 * [\log_{10} CFU/gFW] + 2.8764$. As xylem fluxes of matter depend on the transpiration rate, the upper bound of xylem fluxes was constrained by this transpiration reduction coefficient if the bacterial density was more than 10^7 CFU/gFW.

3. Maximization of the growth of the aerial parts

In this FBA, the pathogen growth rate was now considered as an additional constraint, and leaf/stem biomass reactions were maximized. To this end, maximization of leaf biomass reaction flux was set as objective, and a constant ratio between leaf and stem biomass was imposed to ensure balanced growth of both the stem and the leaves. This FBA determined the growth of the aerial parts still achievable in the presence of *R. pseudosolanacearum*, as the pathogen deprived the plant from a part of its nutrients.

4. Minimization of the sum of absolute fluxes

In this FBA, the leaf/stem growth rates obtained from FBA 3 were set as additional constraints and minimization of all the fluxes was performed. This allowed to consider a parsimonious enzyme usage in both organisms as well as avoid the presence of Stoichiometric Balanced Cycles. This FBA was similarly performed as for the plant model alone (Gerlin et al., 2022).

Simulations were performed with Python 3 scripts, the open access libraries lxml, pandas and the linear programming solver CPLEX Python API, developed by IBM and free for academic institutions.

Data availability

The scripts used to perform all the simulations, as well as the genome-scale metabolic models, can be found on Github at this link: https://github.com/cbaroukh/VIRION [released once accepted].

Author contributions

Caroline Baroukh: Conceptualization (lead); Data curation (equal); Formal analysis (equal); Funding acquisition (lead); Investigation (equal); Methodology (equal); Project administration (lead); Resources (equal); Supervision (lead); Writing – original draft (supporting); Writing – review and editing (equal).

Léo Gerlin: Data curation (equal); Formal analysis (equal); Methodology (equal); Investigation (equal); Writing – original draft (lead); Writing – review and editing (equal).

Stéphane Genin: Conceptualization (supporting); Methodology (supporting); Resources (equal); Writing – review and editing (equal).

Competing interest statement

The authors declare no competing interests.

Funding statement

Léo Gerlin was funded by a PhD grant from the French Ministry of National Education and Research. The study was funded by the French Laboratory of Excellence (LABEX) project TULIP (ANR-10-LABX-41 and ANR11-IDEX-0002-02). The funders had no role in study design, data collection and analysis, decision to publish, or preparation of the manuscript.

Supplementary data

Supplementary Figure 1

R. pseudosolanacearum uptake rates depending on the bacterial density and the limiting factors. g: g of *R. pseudosolanacearum* dry weight. CFU: colony forming units.

Supplementary Text 1

Modifications of tomato metabolic model to build a whole plant – pathogen model.

Supplementary Text 2

Integration of bacterial density in VIRION.

References

Abu Kwaik, Y., & Bumann, D. (2013). Microbial quest for food *in vivo* : 'Nutritional virulence' as an emerging paradigm: Microbial nutritional virulence. *Cellular Microbiology*, *15*(6), 882-890. https://doi.org/10.1111/cmi.12138

Baroukh, C., Gerlin, L., Escourrou, A., & Genin, S. (2024). Unraveling the in planta population dynamics of the plant pathogen Ralstonia pseudosolanacearum by mathematical modeling. *New Phytologist*. https://doi.org/10.1111/nph.20216

Baroukh, C., Zemouri, M., & Genin, S. (2022). Trophic preferences of the pathogen *Ralstonia solanacearum* and consequences on its growth in xylem sap. *MicrobiologyOpen*, *11*(1), e1240. https://doi.org/10.1002/mbo3.1240

Berger, S., Sinha, A. K., & Roitsch, T. (2007). Plant physiology meets phytopathology : Plant primary metabolism and plant pathogen interactions. *Journal of Experimental Botany*, *58*(15-16), 4019-4026. https://doi.org/10.1093/jxb/erm298

Bhatt, G., & Denny, T. P. (2004). *Ralstonia solanacearum* Iron Scavenging by the Siderophore Staphyloferrin B Is Controlled by PhcA, the Global Virulence Regulator. *Journal of Bacteriology*, *186*(23), 7896-7904. https://doi.org/10.1128/JB.186.23.7896-7904.2004

Bialczyk, J., Lechowski, Z., & Dziga, D. (2004). Composition of the xylem sap of tomato seedlings cultivated on media with HCO_3^- and nitrogen source as NO_3 <sup/>—Or NH_4^+. *Plant and Soil*, *263*(1), 265-272. https://doi.org/10.1023/B:PLSO.0000047739.11698.ca

Dalsing, B. L., & Allen, C. (2014). Nitrate Assimilation Contributes to Ralstonia solanacearum Root Attachment, Stem Colonization, and Virulence. *Journal of Bacteriology*, *196*(5), 949-960. https://doi.org/10.1128/JB.01378-13

Dalsing, B. L., Truchon, A. N., Gonzalez-Orta, E. T., Milling, A. S., & Allen, C. (2015). Ralstonia solanacearum Uses Inorganic Nitrogen Metabolism for Virulence, ATP Production, and Detoxification in the Oxygen-Limited Host Xylem Environment. *mBio*, *6*(2), e02471-14. https://doi.org/10.1128/mBio.02471-14

De La Fuente, L., Merfa, M. V., Cobine, P. A., & Coleman, J. J. (2022). Pathogen Adaptation to the Xylem Environment. *Annual Review of Phytopathology*, *60*(1), 163-186. https://doi.org/10.1146/annurev-phyto-021021-041716

diCenzo, G. C., Tesi, M., Pfau, T., Mengoni, A., & Fondi, M. (2020). Genome-scale metabolic reconstruction of the symbiosis between a leguminous plant and a nitrogen-fixing bacterium.

Nature Communications, *11*(1), 2574. https://doi.org/10.1038/s41467-020-16484-2

Gerlin, L., Baroukh, C., & Genin, S. (2021). Polyamines : Double agents in disease and plant immunity. *Trends in Plant Science*, *26*(10), 1061-1071. https://doi.org/10.1016/j.tplants.2021.05.007

Gerlin, L., Cottret, L., Cesbron, S., Taghouti, G., Jacques, M.-A., Genin, S., & Baroukh, C. (2020). Genome-Scale Investigation of the Metabolic Determinants Generating Bacterial Fastidious Growth. *mSystems*, *5*(2), e00698-19. https://doi.org/10.1128/mSystems.00698-19

Gerlin, L., Cottret, L., Escourrou, A., Genin, S., & Baroukh, C. (2022). A multi-organ metabolic model of tomato predicts plant responses to nutritional and genetic perturbations. *Plant Physiology*, *188*(3), 1709-1723. https://doi.org/10.1093/plphys/kiab548

Gerlin, L., Escourrou, A., Cassan, C., Maviane Macia, F., Peeters, N., Genin, S., & Baroukh, C. (2021). Unravelling physiological signatures of tomato bacterial wilt and xylem metabolites exploited by *Ralstonia solanacearum*. *Environmental Microbiology*, *23*(10), 5962-5978. https://doi.org/10.1111/1462-2920.15535

Gerlin, L., Frainay, C., Jourdan, F., Baroukh, C., & Prigent, S. (2021). Plant genome-scale metabolic networks. In *Advances in Botanical Research* (Vol. 98, p. 237-270). Elsevier. https://doi.org/10.1016/bs.abr.2020.09.021

Gu, C., Kim, G. B., Kim, W. J., Kim, H. U., & Lee, S. Y. (2019). Current status and applications of genome-scale metabolic models. *Genome Biology*, *20*(1), 121. https://doi.org/10.1186/s13059-019-1730-3

Hamilton, C. D., Steidl, O. R., MacIntyre, A. M., Hendrich, C. G., & Allen, C. (2021). *Ralstonia solanacearum* Depends on Catabolism of Myo-Inositol, Sucrose, and Trehalose for Virulence in an Infection Stage–Dependent Manner. *Molecular Plant-Microbe Interactions®*, *34*(6), 669-679. https://doi.org/10.1094/MPMI-10-20-0298-R

Herms, D. A., & Mattson, W. J. (1992). The Dilemma of Plants : To Grow or Defend. *The Quarterly Review of Biology*, *67*(3), 283-335. https://doi.org/10.1086/417659

Ingel, B., Caldwell, D., Duong, F., Parkinson, D. Y., McCulloh, K. A., Iyer-Pascuzzi, A. S., McElrone, A. J., & Lowe-Power, T. M. (2022). Revisiting the Source of Wilt Symptoms : X-Ray Microcomputed Tomography Provides Direct Evidence That *Ralstonia* Biomass Clogs Xylem Vessels. *PhytoFrontiers™*, *2*(1), 41-51. https://doi.org/10.1094/PHYTOFR-06-21-0041-R

Lacrampe, N., Lugan, R., Dumont, D., Nicot, P. C., Lecompte, F., & Colombié, S. (2024).

Modelling metabolic fluxes of tomato stems reveals that nitrogen shapes central metabolism for defence against *Botrytis cinerea*. *Journal of Experimental Botany*, *75*(13), 4093-4110. https://doi.org/10.1093/jxb/erae140

Landry, D., González-Fuente, M., Deslandes, L., & Peeters, N. (2020). The large, diverse, and robust arsenal of *Ralstonia solanacearum* type III effectors and their in planta functions. *Molecular Plant Pathology*, *21*(10), 1377-1388. https://doi.org/10.1111/mpp.12977

Lowe-Power, T. M., Hendrich, C. G., Von Roepenack-Lahaye, E., Li, B., Wu, D., Mitra, R., Dalsing, B. L., Ricca, P., Naidoo, J., Cook, D., Jancewicz, A., Masson, P., Thomma, B., Lahaye, T., Michael, A. J., & Allen, C. (2018). Metabolomics of tomato xylem sap during bacterial wilt reveals *Ralstonia solanacearum* produces abundant putrescine, a metabolite that accelerates wilt disease. *Environmental Microbiology*, *20*(4), 1330-1349. https://doi.org/10.1111/1462-2920.14020

Lowe-Power, T. M., Khokhani, D., & Allen, C. (2018). How Ralstonia solanacearum Exploits and Thrives in the Flowing Plant Xylem Environment. *Trends in Microbiology*, *26*(11), 929-942. https://doi.org/10.1016/j.tim.2018.06.002

Macho, A. P. (2016). Subversion of plant cellular functions by bacterial type- III effectors : Beyond suppression of immunity. *New Phytologist*, *210*(1), 51-57. https://doi.org/10.1111/nph.13605

MacIntyre, A. M., Barth, J. X., Pellitteri Hahn, M. C., Scarlett, C. O., Genin, S., & Allen, C. (2020). Trehalose Synthesis Contributes to Osmotic Stress Tolerance and Virulence of the Bacterial Wilt Pathogen *Ralstonia solanacearum*. *Molecular Plant-Microbe Interactions®*, *33*(3), 462-473. https://doi.org/10.1094/MPMI-08-19-0218-R

Orth, J. D., Thiele, I., & Palsson, B. Ø. (2010). What is flux balance analysis? *Nature Biotechnology*, *28*(3), 245-248. https://doi.org/10.1038/nbt.1614

Peyraud, R., Cottret, L., Marmiesse, L., & Genin, S. (2018). Control of primary metabolism by a virulence regulatory network promotes robustness in a plant pathogen. *Nature Communications*, *9*(1), 418. https://doi.org/10.1038/s41467-017-02660-4

Peyraud, R., Cottret, L., Marmiesse, L., Gouzy, J., & Genin, S. (2016). A Resource Allocation Trade-Off between Virulence and Proliferation Drives Metabolic Versatility in the Plant Pathogen Ralstonia solanacearum. *PLoS Pathogens*, *12*(10), e1005939. https://doi.org/10.1371/journal.ppat.1005939

Rodenburg, S. Y. A., Seidl, M. F., Judelson, H. S., Vu, A. L., Govers, F., & De Ridder, D.

(2019). Metabolic Model of the *Phytophthora infestans* -Tomato Interaction Reveals Metabolic Switches during Host Colonization. *mBio*, *10*(4), e00454-19. https://doi.org/10.1128/mBio.00454-19

Roper, C., Castro, C., & Ingel, B. (2019). Xylella fastidiosa : Bacterial parasitism with hallmarks of commensalism. *Current Opinion in Plant Biology*, *50*, 140-147. https://doi.org/10.1016/j.pbi.2019.05.005

Vailleau, F., & Genin, S. (2023). *Ralstonia solanacearum* : An Arsenal of Virulence Strategies and Prospects for Resistance. *Annual Review of Phytopathology*, *61*(1), 25-47. https://doi.org/10.1146/annurev-phyto-021622-104551

Walters, D., & Heil, M. (2007). Costs and trade-offs associated with induced resistance. *Physiological and Molecular Plant Pathology*, *71*(1-3), 3-17. https://doi.org/10.1016/j.pmpp.2007.09.008

Yuan, H., Cheung, C. Y. M., Poolman, M. G., Hilbers, P. A. J., & Van Riel, N. A. W. (2016). A genome-scale metabolic network reconstruction of tomato (*Solanum lycopersicum* L.) and its application to photorespiratory metabolism. *The Plant Journal*, *85*(2), 289-304. https://doi.org/10.1111/tpj.13075

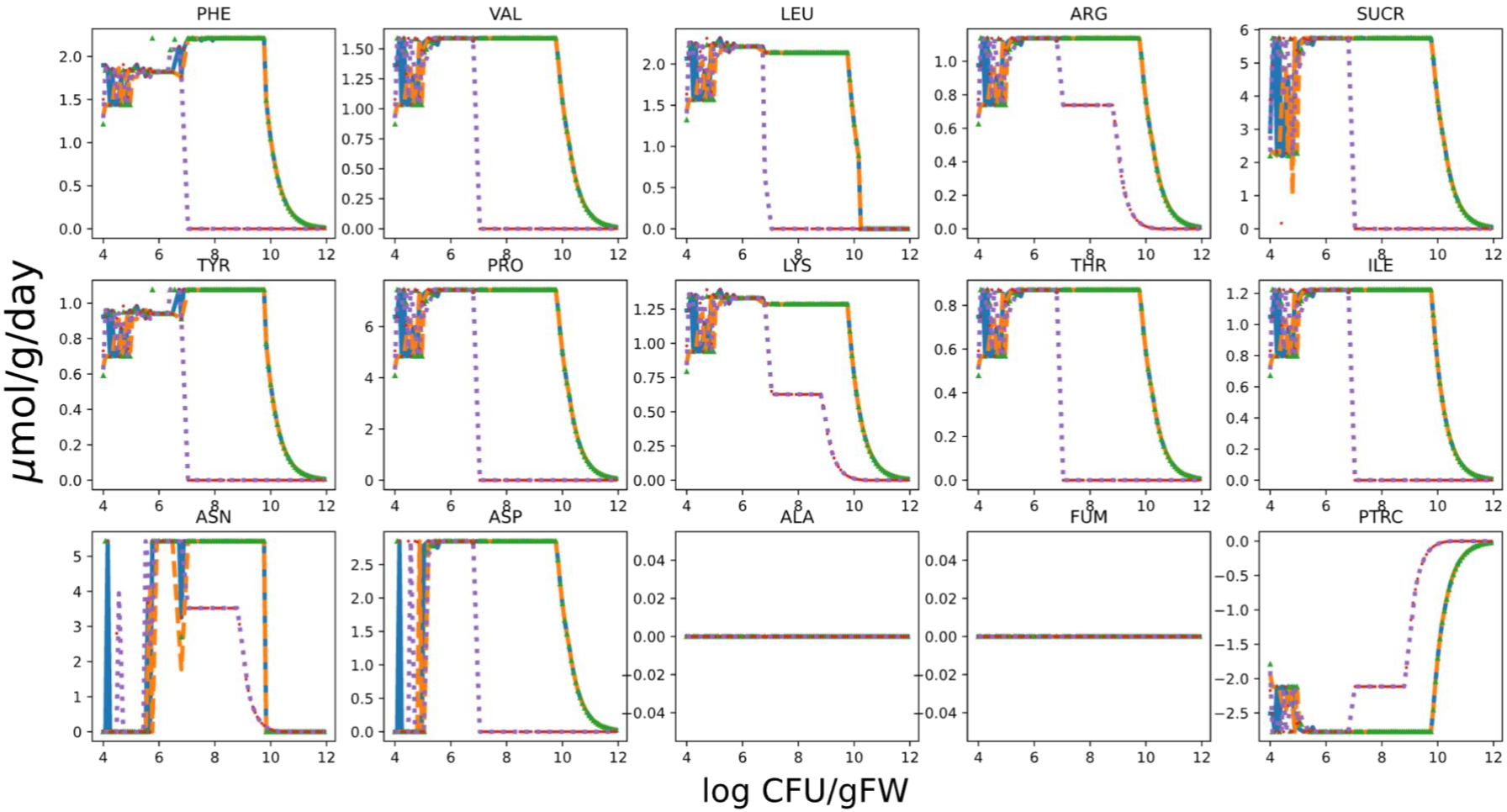

Supplementary figure 1: *R. pseudosolanacearum* uptake rates depending on the bacterial density and the limiting factors. g: g of *R. pseudosolanacearum* dry weight. CFU: colony forming units.

Modifications of tomato metabolic model to build a whole plant – pathogen model

1. Determination of iron concentration in tomato plant from literature for integration in biomass

Iron was initially absent from tomato biomass. Regarding its importance in plant – *Ralstonia* interaction (ref), we added it to organ biomass reactions (R_BIOMASS_ROOT, R_BIOMASS_STEM, R_BIOMASS_LEAF). We determined the coefficient value in the equation following the procedure below.

- **From Twyman, 1959 [1]**

Mean concentration of iron in dry leaf tissue of tomato plants:
[Fe] = 144 ppm at the highest iron supply (Table 2)
[Fe] = 144 ppm = 144 mg Fe/kg leaf DW

Note: at the lowest iron supply, the value remains close (112 mg Fe/kg leaf DW).

- **From Carpena et al., 1988 [2]**

Cultivar	Vermone	Marglobe
Nutrient consumption (mg Fe/plant) – Table 3	301	298
Yield, plant weight (g/plant) – Table 4	3054	2613
Yield, fruit weight (g/plant) – Table 4	6648	3930
Yield, plant dry weight (g DW/plant)*	432	370
Yield, fruit dry weight (g DW/plant)**	398	235
Total dry weight (g DW/plant)	830	605
Total dry weight (kg DW/plant)	0.830	0.733
[Fe] (mg Fe/kg DW)* **	**363**	**406.5**

*Using FW/DW ratio of 7.07 according to Gerlin et al., 2022 [3]

**Using FW/DW ratio of 16.7 (6% of dry content) [4]

***[Fe] (mg Fe/kg DW) = Nutrient consumption (mg Fe/plant)/Total dry weight (kg DW/plant)

➔ Integration of iron concentration in tomato model

The range estimated from literature is **144 – 406.5 mg Fe/kg DW** in a tomato plant.
Biomass equation represents 1 g of organ DW, corresponding to 1.44 – 4.07 10^{-4} g Fe.
Using the atomic weight of Fe (55.845 g/mol), it represents 2.58 – 7.28 10^{-6} mol Fe.
Biomass equation is expressed in µmol/gDW, so the range of values to integrate in the model is: **2.58 – 7.28 µmol/gDW.** Iron is majorly found in and between plant organs as Fe2+ (M_fe2_c) [5], so iron will be incorporated in biomass equation as M_fe2_c (see reference below).
Here, we do not take into account the organ specificity of iron concentration and add the same value in leaf, stem and root. We integrate the highest value to mimic a maximal requirement. Simulations presented in the paper show that even this high value has poor impact on the interaction.

2. Addition of minerals required for pathogen growth

Molybdate (M_mobd_c), manganese (M_mn_c) and cobalt (M_cobalt_c) are present in *R. pseudosolanacearum* biomass equation while they were not modeled in plant initial metabolic model (Sl2183).
We added:

- **For molybdate**

The internal metabolite M_mobd_c was already present. We added the boundary metabolite M_mobd_b and the uptake reaction R_EX_mobd_c, written as follow:
M_mobd_b <-> M_mobd_c

- **For manganese**

We added the internal and boundary metabolites M_mn2_b and M_mn2_c and the uptake reaction R_EX_mn2_c, written as follow:
M_mn2_b <-> M_mn2_c

- **For cobalt**

We added the internal and boundary metabolites M_cobalt2_b and M_cobalt2_c and the uptake reaction R_EX_cobalt2_c, written as follow:
M_ cobalt2_b <-> M_ cobalt2_c

3. Corrections of amino acid coefficients in biomass equation

The coefficients for some amino acids were inverted in the previous files of tomato model published in 2022 [3]. While it does not have significant impact on the simulations, either here or in the previous work, we rewrote the coefficients for the following amino acids: M_cys__L_c, M_ala__B_c, M_his__L_c, M_ile__L_c, M_leu__L_c, M_lys__L_c with the correct values from the list of biomass components (Supp File 1 of Gerlin et al. 2022 [3], sheets 3, 4, 5).

4. Putrescine metabolism

We manually examined putrescine catabolism in Sl2183, as our initial model was not representing putrescine catabolism. We looked at canonical putrescine catabolism in plants in literature [6] and databases (https://pmn.plantcyc.org/pathway?orgid=ARA&id=PWY-2).
We found that the first reaction of putrescine catabolism, putrescine oxidase* (EC 1.4.3.10) was already included in our model (converting putrescine into 4-aminobutanoate), but we missed the following reaction, aminobutyraldehyde dehydrogenase** (EC 1.2.1.19), converting 4-aminobutanoate into GABA. We found two orthologs (SOLYC06G071290 OR SOLYC03G113800) to the A. thaliana gene (ALDH10A9 / AT3G48170) annotated as aminobutyraldehyde dehydrogenase in BioCyc. This provides evidence for the completeness of the pathway in tomato, and we thus added aminobutyraldehyde dehydrogenase in the modeL

*Putrescine oxidase
R_PTRCOX1 http://bigg.ucsd.edu/universal/reactions/PTRCOX1 in BiGG
PUTRESCINE-OXIDASE-RXN https://biocyc.org/reaction?orgid=META&id=PUTRESCINE-OXIDASE-RXN in BioCyc
Reaction in BiGG: M_h2o_c + M_o2_c + M_ptrc_c -> M_4abutn_c + M_h2o2_c + M_nh4_c

**Aminobutyraldehyde dehydrogenase
R_ABUTD http://bigg.ucsd.edu/models/iJO1366/reactions/ABUTD in BiGG
AMINOBUTDEHYDROG-RXN https://biocyc.org/reaction?orgid=META&id=AMINOBUTDEHYDROG-RXN in BioCyc
Reaction in BiGG: M_4abutn_c + M_h2o_c + M_nad_c -> M_4abut_c + 2.0 M_h_c + M_nadh_c

References

[1] E. S. Twyman, « The effect of iron supply on the yield and composition of leaves of tomato plants », *Plant Soil*, vol. 10, nº 4, p. 375-388, avr. 1959, doi: 10.1007/BF01666211.
[2] O. Carpena, A. Masaguer, et M. J. Sarro, « Nutrient uptake by two cultivars of tomato plants », *Plant Soil*, vol. 105, nº 2, p. 294-296, sept. 1988, doi: 10.1007/BF02376796.
[3] L. Gerlin, L. Cottret, A. Escourrou, S. Genin, et C. Baroukh, « A multi-organ metabolic model of tomato predicts plant responses to nutritional and genetic perturbations », *Plant Physiol.*, vol. 188, nº 3, p. 1709-1723, mars 2022, doi: 10.1093/plphys/kiab548.
[4] E. Cozzolino *et al.*, « Effects of the Application of a Plant-Based Compost on Yield and Quality of Industrial Tomato (Solanum lycopersicum L.) Grown in Different Soils », *Appl. Sci.*, vol. 13, nº 14, p. 8401, juill. 2023, doi: 10.3390/app13148401.
[5] J.-F. Briat, C. Curie, et F. Gaymard, « Iron utilization and metabolism in plants », *Curr. Opin. Plant Biol.*, vol. 10, nº 3, p. 276-282, juin 2007, doi: 10.1016/j.pbi.2007.04.003.
[6] R. Rastogi et P. J. Davies, « Polyamine Metabolism in Ripening Tomato Fruit 1: I. Identification of Metabolites of Putrescine and Spermidine », *Plant Physiol.*, vol. 94, nº 3, p. 1449-1455, nov. 1990, doi: 10.1104/pp.94.3.1449.

Integration of bacterial density in VIRION

Numerical values used

$1.0157 \cdot 10^{12}$ CFU *Rs*/L = 1 OD	Value from (Peyraud et al., 2016) Linear regression from S4 Table.
0.414 g *Rs*/L = 1 OD	Value from (Peyraud et al., 2016) Materials and Methods.
g fresh weight / g dry weight [*Sl* stem] = 17.7	Value from (Gerlin et al., 2022) Figure 2.

g / CFU [*Rs*] = 0.414 g *Rs*/L / $1.0157 \cdot 10^{12}$ CFU *Rs*/L = $4.076 \cdot 10^{-13}$

1 cfu/g stem FW = 1·(g fresh weight / g dry weight [*Sl* stem]) = 17.7 **cfu/g stem DW**

In VYTOP model, the relative proportions are: 1.52 g stem DW and 3.37 g leaf DW for 1 g root DW. The bacterial density must be determined for 1.52 g stem DW.

1 cfu/g stem FW = 1.52 · 17.7 **cfu/1.52 g stem DW** = 26.904 **cfu/1.52 g stem DW**
1 cfu/g stem FW = 26.904 · (g / CFU [*Rs*]) **g bact / 1.52 g stem DW**
1 cfu/g stem FW = $26.904 \cdot 4.076.10^{-13}$ **g bact / 1.52 g stem DW**
1 cfu/g stem FW = $1.10 \cdot 10^{-11}$ **g bact / 1.52 g stem DW**

Rs: *Ralstonia pseudosolanacearum* GMI1000
Sl: *Solanum lycopersicum* M80

References

Peyraud R, Cottret L, Marmiesse L, Gouzy J, Genin S. A Resource Allocation Trade-Off between Virulence and Proliferation Drives Metabolic Versatility in the Plant Pathogen Ralstonia solanacearum. PLoS Pathog. 2016 Oct 12;12(10):e1005939. doi: 10.1371/journal.ppat.1005939. PMID: 27732672; PMCID: PMC5061431.

Gerlin L, Cottret L, Escourrou A, Genin S, Baroukh C. A multi-organ metabolic model of tomato predicts plant responses to nutritional and genetic perturbations. Plant Physiol. 2022 Mar 4;188(3):1709-1723. doi: 10.1093/plphys/kiab548. PMID: 34907432; PMCID: PMC8896645.